Figure 5 displays the temperature dependence of the field-cooled (Meissner effect) and zero-field-cooled (shielding effect) magnetization for C4 measured in a field of 100 Oe between 5 and 130 K with a SQUID magnetometer. As shown in Figure 5, a superconducting transition at $T_0 = 110$ K is observed, which is consistent with the resistance measurement. A small amount of 80 K phase is seen coexisting with the 110 K phase. The estimated Meissner fraction is about 30%.

Figure 6 shows the XRD pattern for C4. The major peaks belong to $(Bi,Pb)_2Sr_2Ca_2Cu_3O_y$ ($T_c = 110$ K) with a small amount of $(Bi,Pb)_2Sr_2CaCu$ ($T_c = 80$ K) and an impurity phase of Ca_2PbO_4.[8,9]

(8) Murayama, N.; Sudo, E.; Awano, M.; Kani, K.; Torri, Y. *Jpn. J. Appl. Phys.* **1988**, *27*, L1629.
(9) Oota, A.; Sasaki, Y.,; Kirihigashi, A. *Jpn. J. Appl. Phys.* **1988**, *27*, L1445.

Conclusion

A high-T_c superconducting oxide powder of Bi(Pb)-Sr-Ca-Cu-O has been prepared by means of coprecipitation using Bi, Pb, Sr, Ca, and Cu nitrates as starting materials with oxalic acid/triethylamine as a precipitant. Fine, homogeneous stoichiometric powders were obtained by using optimum $Et_3N/H_2C_2O_4$ ratios between 1.5 to 2.2. Subsequent calcination at 800 °C for 10 h and sintering at 860 °C for 72 h are recommended for the 110 K Bi-base superconductor. All the experimental conditions can be easily controlled and reproduced. This technique has great potential for a scale-up production.

Acknowledgment. This work was partially supported by the National Science Council.

Registry No. $Bi(NO_3)_3$, 10361-44-1; $Pb(NO_3)_2$, 10099-74-8; $Sr(NO_3)_2$, 10042-76-9; $Ca(NO_3)_2$, 10124-37-5; $Cu(NO_3)_2$, 3251-23-8; Et_3N, 121-44-8; $H_2C_2O_4$, 144-62-7; $(Bi,Pb)_2Sr_2Ca_2Cu_3O_4$, 116739-98-1.

Contribution from the Department of Physics, Clark University, Worcester, Massachusetts 01610-1477, and Department of Chemistry, Northeastern University, Boston, Massachusetts 02115

A Bromide Analogue of a One-Dimensional Ising Ferromagnet: Trimethylammonium *catena*-Bis(μ-bromo)diaquoiron(II) Bromide

R. E. Greeney,[†,§] C. P. Landee,*[,†] J. H. Zhang,[‡,∥] and W. M. Reiff*[,‡]

Received September 6, 1989

The crystal structure of the title compound, FeTAB, has been determined by X-ray diffraction and has been found to be isomorphous to that of the chloride analogue, FeTAC. The structure consists of chains of bibromide-bridged Fe^{2+} ions extending along the *b* axis of the orthorhombic unit cell (space group *Pnma*, $a = 17.287$ (3) Å, $b = 7.651$ (2) Å, $c = 8.320$ (3) Å, $R(F_o) = 0.0494$, $R_w(F_o) = 0.0488$). The chains are linked into a 2-dimensional network in the *c* direction by hydrogen bonding to a third bromide ion; the resulting planes are well isolated in the *a* direction by the organic molecules. The low-temperature magnetic susceptibility of polycrystalline samples can be modeled by using a one-dimensional ferromagnetic Ising model with a molecular field correction. The exchange parameters are estimated to be $J/k = 4$ K and $z'J'/k = -0.2$ K, indicating that FeTAB has an intrachain exchange constant only one-fourth of that found in the chloride analogue while the interchain interactions are more than 10-times greater. Antiferromagnetic ordering is observed in the Mössbauer spectra near 1.3 K. Analysis of the polycrystalline spectra shows that the internal magnetic field (and easy axis of magnetization) for FeTAB lies close to the *ab* plane, as previously found for FeTAC.

Introduction

The series of isostructural 3d M(II) linear-chain compounds $[(CH_3)_3NH]MCl_3 \cdot 2H_2O$ (abbreviated as MTAC), for M = Mn, Fe, Co, Ni, and Cu, has been thoroughly studied.[1-11] All of the compounds consist of dichloro-bridged chains of M^{2+} ions, held together into layers by hydrogen bonding to a noncoordinated chloride ion. The resulting layers are well separated by the bulk of the trimethylammonium ions. Magnetic studies have shown the magnetic interactions to reflect the structural anisotropy, these compounds possessing a pronounced one-dimensional character. The interactions between adjacent chains are normally only a few percent of that of the intrachain exchange, although in FeTAC the magnetic isolation has recently been shown[5] to be a factor of 10 better. The low-dimensional character causes the magnetic ordering temperatures to occur in the liquid-helium temperature region.

The ability of this structure to include all of the 3d metal ions from manganese to copper presents a valuable framework in which to study both the effects of the number of 3d electrons in the magnetic ion upon magnetic behavior and to study the magnetic behavior of mixed-metal systems. Examination of the pure compounds has shown that the dominant, intrachain interactions are ferromagnetic for all the members of the MTAC family, with the exception of MnTAC. The manganese[2-4] and nickel[8,9] compounds have been found to behave as essentially Heisenberg linear chains, although single-ion effects are not negligible. The cobalt[6,7] and ferrous[5] compounds are Ising systems, with spin canting present in CoTAC, which causes it to order as a weak ferromagnet. The copper compound was the first reported example of a ferromagnetic $S = {}^1/_2$ Heisenberg linear chain.[10] There is, however, a significant amount of both Ising component in the exchange interaction and interchain exchange present in this compound, which lead to both spin dimensionality and lattice dimensionality crossovers at low temperature.[11]

* To whom correspondence should be addressed.
† Clark University.
‡ Northeastern University.
§ Present address: Maryville College, Maryville, TN 37801.
∥ Present address: Department of Chemistry, University of New Orleans, New Orleans, LA 70148.

(1) Caputo, R. E.; Willett, R. D.; Muir, J. A. *Acta Crystallogr., B* **1976**, *32*, 2639. Depmeier, W.; Klaska, K. H. *Acta Crystallogr., B* **1976**, *36*, 1065.
(2) Merchant, S.; McElearney, J. N.; Shankle, G. E.; Carlin, R. L. *Physica* **1974**, *78*, 308.
(3) Takeda, K.; Koike, T.; Harada, I.; Tonegawa, T. *J. Phys. Soc. Jpn.* **1982**, *51*, 85.
(4) Yamamoto, I.; Nagata, K. *J. Phys. Soc. Jpn.* **1977**, *43*, 1581.
(5) Greeney, R. E.; Landee, C. P.; Zhang, J. H.; Reiff, W. M. *Phys. Rev. B: Condens. Matter* **1989**, *39*, 12200.
(6) Losee, D. B.; McElearney, J. N.; Shankle, G. E.; Carlin, R. L.; Cresswell, P. J.; Robinson, W. T. *Phys. Rev. B: Condens. Matter* **1973**, *8*, 2185.
(7) Groenendijk, H. A.; van Duyneveldt, A. J. *Physica B + C* **1982**, *115*, 41.
(8) O'Brien, S.; Gaura, R. M.; Landee, C. P.; Willett, R. D. *Solid State Commun.* **1981**, *39*, 1333.
(9) Hoogerbeets, R.; Wiegers, S. A. J.; van Duyneveldt, A. J.; Willett, R. D.; Geiser, U. *Physica B + C* **1984**, *125*, 135.
(10) Losee, D. B.; McElearney, J. N.; Siegel, A.; Carlin, R. L.; Khan, A. A.; Roux, J. P.; James, W. P. *Phys. Rev. B: Condens. Matter* **1972**, *6*, 4342. Babst, I.; Bats, J. W. *Acta Crystallogr., C* **1985**, *41*, 1297.
(11) Algra, H. A.; de Jongh, L. J.; Huiskamp, W. J.; Carlin, R. L. *Physica* **1977**, *92B*, 187.

0020-1669/90/1329-3119$02.50/0

Table I. Crystallographic Data for FeTAB

compound name: trimethylammonium
catena-bis(μ-bromo)diaquorion(II) bromide
empirical formula: $C_3H_{14}Br_3FeNO_2$
fw = 391.72
space group: *Pnma* (No. 62)
temp: ambient
a = 17.287 (3) Å
b = 7.651 (2) Å
c = 8.320 (3) Å
V = 1100.5 (4) Å^3
Z = 4
λ = 0.71069 Å
abs coeff (μ) = 121.22 cm^{-1}
ρ_{calc} = 2.35 g cm^{-3}
transm coeff = 0.549–0.788
$R(F_o)$ = 0.0494 (0.0686, all reflcns)
$R_w(F_o)$ = 0.0488 (0.5948 all reflcns)

The MTAC family has already been the subject of a number of experiments on mixed-metal systems, in which a second metal ion is doped randomly into the chain. Studies have been made on the mixtures (Mn/Cu)TAC,[12] (Mn/Co)TAC,[13-15] (Mn/Ni)TAC,[15] and (Co/Ni)TAC.[15]

Much less attention has been given to the question of the effect of halide substitution in this family of compounds. It is known that the analogous bromide compounds (MTAB) exist for at least the manganese[2,4] and cobalt[16] cases. However, none of the structures of the MTAB compounds have been determined, and only the magnetic properties of MnTAB have been reported in detail. Since the substitution of bromide for chloride ions is known[17] to have strong effects upon both the magnetic exchange and the magnetic anisotropy in copper halide compounds, it is worth examining the effects of such substitution upon the magnetic behavior of 3d metal ions with more than one magnetic electron. We present here the results of the structural determination of the ferrous bromide member of this series, FeTAB, as well as of magnetic susceptibility and Mössbauer spectroscopy experiments on polycrystalline samples. A preliminary report of these results has appeared elsewhere.[18]

Experimental Section

A. Sample Preparation. Samples of FeTAB were prepared by dissolving iron powder in 3 M HBr and adding equimolar amounts of trimethylammonium bromide. The solution was allowed to evaporate slowly at room temperature in a desiccator under nitrogen atmosphere. All handling and storage was done under inert atmosphere since FeTAB, unlike FeTAC, is quite prone to oxidation, particularly above room temperature. Allowing the solution to evaporate in a cold room (5 °C) was found to be of only marginal utility.

The nearly transparent crystals grow elongated along the b (chain) axis. The chemical formula of the title compound was confirmed by commercial chemical analysis. A second phase consisting of reddish platelike crystals sometimes coprecipitates with the FeTAB; it has not yet been identified.

B. X-ray Structural Determination. The X-ray structural determination was performed in the laboratory of Professor R. D. Willett of Washington State University using an upgraded Syntex P2$_1$ diffractometer system. The crystal studied (dimensions 0.18 × 0.28 × 0.42 mm) was kept in a capillary during data collection. The system is orthorhombic, *Pnma*, with a = 17.287 (3) Å, b = 7.651 (2) Å, c = 8.320 (3) Å, and Z = 4 with ρ_{calc} = 2.35 g/cm^3. Molybdenum Kα radiation was used with a graphite monochrometer (λ = 0.71069 Å). No decays were observed in the standard reflections during data collection. Empirical absorption corrections were made, using an absorption coefficient of 121.22 cm^{-1}. On the basis of the similarities of the space group and lattice parameters to those of FeTAC,[5] starting positions for non-hydrogen atoms were assumed to be the same as found in the chloride analogue. Following a successful initial refinement, hydrogen atoms were added. The positions for all hydrogen atoms, other than the C(1) methyl group, were calculated. The bond lengths were constrained to 0.960 Å, and bond angles were fixed at 109.5°. The isotropic thermal parameters were fixed at 1.2 times the equivalent isotropic thermal parameters of the atoms they were bonded to. The positions of the hydrogen atoms on C(1) were determined from the Fourier map. The positions were refined with constraints to insure approximate tetrahedral symmetry. The isotropic thermal parameters were fixed at 0.05. All refinements were accomplished with use of the version 4.1 SHELXTL programs.[19] A final value of $R = \sum||F_o| - |F_c||/\sum|F_o| = 0.0494$ and $R_w = (\sum w(F_o - F_c)^2/\sum w|F_o|^2)^{1/2} = 0.0488$ was obtained.

Data collection parameters are given in Table I, and final positional and isotropic thermal parameters are given in Table II, with selected bond lengths and angles given in Table III. A fuller set of hydrogen atom positional and isotropic thermal parameters, anisotropic thermal parameters for non-hydrogen atoms, and $|F_o|$ and $|F_c|$ values are available as supplementary materials.

C. Magnetic and Mössbauer Measurements. Magnetic measurements were made by using a PAR Model 155 vibrating sample magnetometer and a custom helium cryostat.[20] Field and temperature measurements above 1.8 K were made by using calibrated Hall probes and carbon-glass resistance thermometers, respectively. For temperatures below 1.8 K, the

Table II. Fractional Coordinates (×10^4) and Equivalent Isotropic Thermal Parameters (Å^2 × 10^3) for $[(CH_3)_3NH]FeBr_3\cdot 2H_2O$

atom	x	y	z	U_{eq}[a]
Fe	0	0	0	19 (1)
Br(1)	−1033 (1)	2500	14 (1)	21 (1)
Br(2)	1022 (1)	2500	−827 (2)	24 (1)
Br(3)	−879 (1)	2500	4992 (2)	28 (1)
O	247 (3)	432 (7)	2450 (6)	24 (1)
N	1827 (5)	2500	2993 (11)	27 (3)
C(1)	1662 (8)	2500	4756 (16)	38 (4)
C(2)	2253 (5)	947 (11)	2511 (11)	40 (3)

[a] The equivalent isotropic U is defined as one-third of the trace of the orthogonalized U_{ij} tensor.

Table III. Bonding Parameters for $[(CH_3)_3NH]FeBr_3\cdot 2H_2O$[a]

	(a) Bond Lengths (Å)		
Fe–Br(1)	2.617 (1)	N–C(1)	1.495 (16)
Fe–Br(2)	2.693 (1)	N–C(2)	1.454 (10)
Fe–O	2.109 (5)		
	(b) Bond Angles (deg)		
Br(1)–Fe–Br(2)	86.0 (1)	Br(1)–Fe–O	90.8 (2)
Fe–Br(1)–Fe(a)	93.9 (1)		
Br(2)–Fe–O	90.1 (1)	Fe–Br(2)–Fe(a)	90.5 (1)

[a] Fe(a) is the symmetry-related ferrous ion in the chain.

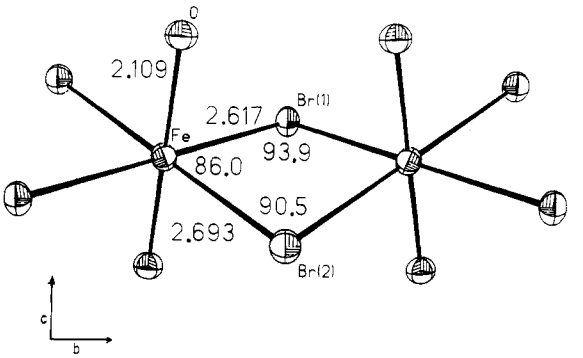

Figure 1. Chain structure of FeTAB. Bond distances are given in angstroms, with bond angles in degrees. The chains run along the b axis. The Fe–O bonds make an angle of 14.8° with the c axis (vertical).

(12) Shouten, J. C.; Taketa, K.; Kopinga, K. *J. Phys. C* **1978**, *6*, 723.
(13) Phaff, A. C.; Swüste, C. H. W.; de Jongh, W. J. M. *Phys. Rev. B: Condens. Matter* **1982**, *25*, 6570.
(14) Cheikrouhou, A.; Dupas, C.; Renard, J.-P.; Veillet, P. *J. Magn. Magn. Mater.* **1985**, *49*, 201.
(15) Rubenacker, G. V.; Raffaelle, D. P.; Drumheller, J. E.; Emerson, K. *Phys. Rev. B: Condens. Matter* **1988**, *37*, 3563.
(16) Carlin, R. L. *Magnetochemistry*; Springer-Verlag: Berlin, Heidelberg, FRG, New York, Tokyo, 1986; p 218.
(17) Willett, R. D. *Inorg. Chem.* **1986**, *25*, 1918.
(18) Greeney, R. E.; Landee, C. P.; Reiff, W. M.; Zhang, J. H. *J. Appl. Phys.* **1988**, *64*, 5938.
(19) Sheldrick, G. *SHELXTL*, Version 4.1; Nicolet Analytical Instruments: Madison, WI, 1984.
(20) Landee, C. P.; Greeney, R. E.; Lamas, A. C. *Rev. Sci. Instrum.* **1987**, *58*, 1957.

Table IV. Structural Parameters for Orthorhombic Members of the Series $[(CH_3)_3N]MX_3 \cdot 2H_2O$ (M = Metal, X = Cl, Br)[f]

param	MnTAC	FeTAC	FeTAB	CoTAC	NiTAC
a, Å	16.779	16.711	17.287	16.671	16.677
b, Å	7.434	7.361	7.651	7.273	7.169
c, Å	8.198	8.140	8.320	8.113	8.103
M–X(1), Å	2.524	2.485	2.617	2.456	2.415
M–X(2), Å	2.581	2.544	2.693	2.503	2.464
M–O, Å	2.186	2.113	2.109	2.078	2.056
X(1)–M–X(2), deg	85.28	84.6	86.0	84.49	84.29
M–X(1)–M(a), deg	94.83	95.5	93.9	95.52	95.84
M–X(2)–M(a), deg	92.13	92.7	90.5	93.14	93.35
X(1)–X(2), Å	3.485	3.385	3.622	3.334	3.273
M–M, Å	3.718	3.680	3.825	3.618	3.584
dihedral fold, deg	16.20	16.3	19.8	15.58	15.26
ref	*a*	*b*	*c*	*d*	*e*

[a] Caputo, R. E.; Willett, R. D.; Muir, J. A. *Acta Crystallogr., B* **1976**, *32*, 2639. [b] Greeney, R. E.; Landee, C. P.; Zhang, J. H.; Reiff, W. M. *Phys. Rev. B: Condens. Matter* **1989**, *39*, 12200. [c] This work. [d] Losee, D. B.; McElearney, J. N.; Shankle, G. E.; Carlin, R. L.; Cresswell, P. J.; Robinson, W. T. *Phys. Rev. B: Condens. Matter* **1973**, *8*, 2185. [e] Hoogerbeets, R.; Wiegers, S. A. J.; van Duyneveldt, A. J.; Willett, R. D.; Geiser, U. *Physica B + C* **1984**, *125*, 135. [f] M(a) is the symmetry-related metal ion in the chain.

samples were immersed directly in liquid helium and the temperature derived from the ^{4}He vapor pressure scale.

Mössbauer spectra of polycrystalline samples of FeTAB have been measured between 0.4 and 300 K in zero applied field. Spectra above 1.6 K were collected on a conventional constant acceleration spectrometer operated in horizontal geometry. The source was ^{57}Co (100 mCi) diffused into a Rh matrix held at room temperature. The temperature of the sample was varied in a flow-type helium-4 cryostat and was determined by using either a calibrated silicon diode and/or vapor pressure thermometry. Spectra measured below 1.6 K were determined with a closed-cycle carbon sorption pumped ^{3}He cryostat.[21]

Results and Discussion

Structural Description. As in the corresponding chloride salts of manganese,[1] iron,[5] cobalt,[6] nickel,[9] and copper,[10] FeTAB forms chains of edge-sharing octahedra [*trans*-$FeBr_4(H_2O)_2$] along the crystallographic *b* axis. The ferrous ion is situated on a center of inversion with the two bridging bromide ions on a mirror plane normal to the chain (Figure 1). Structural parameters of all orthorhombic members of the TAC/TAB family are compared in Table IV. It is seen that among the chloride members the metal–chloride and metal–oxygen bond lengths decrease steadily across the table; these trends are consistent with the decrease in ionic radii in going from Mn^{2+} to Ni^{2+}. Similarly, the internal Cl(1)–M–Cl(2) angles decrease from 85.28° (Mn) to 84.29° (Ni) as the bridging M–Cl–M angles increase from 94.83 and 92.13° (Mn) to 95.84 and 93.35° (Ni). The effect of the alteration of angle plus the decrease in the M–M distance means the Cl(1)–Cl(2) distance shortens severely: 3.485 Å (Mn), 3.385 Å (Fe), 3.334 Å (Co), and 3.273 Å (Ni).

The structural differences between FeTAB and that of the corresponding chloride FeTAC are slight and, with one exception, attributable to the difference of the halide radii. The effect of bromide substitution is to increase the two Fe–halide bond distances by 0.132 and 0.149 Å, consistent with the larger ionic radius of the bromide ion (1.95 Å, Br–; 1.80 Å, Cl–). Compared to the angles in FeTAC, the internal X(1)–Fe–X(2) angle is 1.4° larger at 86.0° while the two bridging angles are 1.6 and 2.2° smaller at 93.9 and 90.5°, respectively. These changes create both the largest metal–metal distance in the series (3.825 Å) and the largest X(1)–X(2) separation at 3.622 Å. The $FeBr_4(H_2O)_2$ octahedra are alternately tilted from the *b* axis by ±9.9°, leading to a dihedral fold angle between adjacent $FeBr_4$ planes of 19.8°, 3.3° larger than that found in FeTAC.

Adjacent chains are connected in the *c* direction by hydrogen bonds involving the water ligand and the uncoordinated bromide, Br(3) (Figure 2). The separation between chains is 8.320 Å for FeTAB, 0.18 Å greater than the value found in FeTAC, yet significantly smaller than the increase of 0.6 Å expected solely on the basis of the increase of ionic radii. The impact of this separation upon the interchain magnetic exchange is discussed later. The chains are positioned in the *bc* plane such that the Fe–O bonds are tilted by 14.8° above or below the *c* axis; this corresponds to a rotation of the chains slightly greater than that found in FeTAC (tilt angle = 12.7°). The hydrogen bonds provide a weak superexchange pathway between the chains, which ties the chains magnetically into sheets. The trimethylammonium ions are located between the sheets and provide good magnetic isolation. The lattice parameter in the *a* direction (17.287 Å) is 0.576 Å greater than the corresponding FeTAC value but consistent with the presence of the two layers of bromide ions in the unit cell, each 0.3 Å larger in diameter than the corresponding chloride.

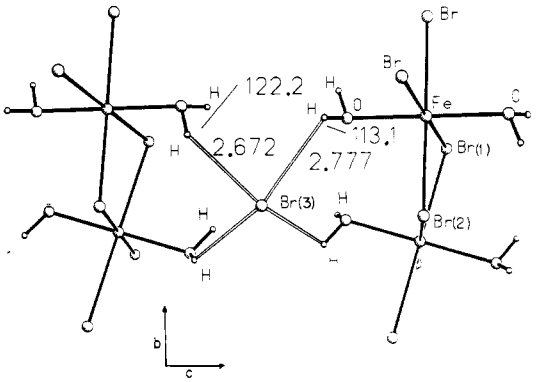

Figure 2. Hydrogen bonding in FeTAB. The chains along the *b* axis are linked together by hydrogen bonds from the water molecules to the lattice bromide Br(3).

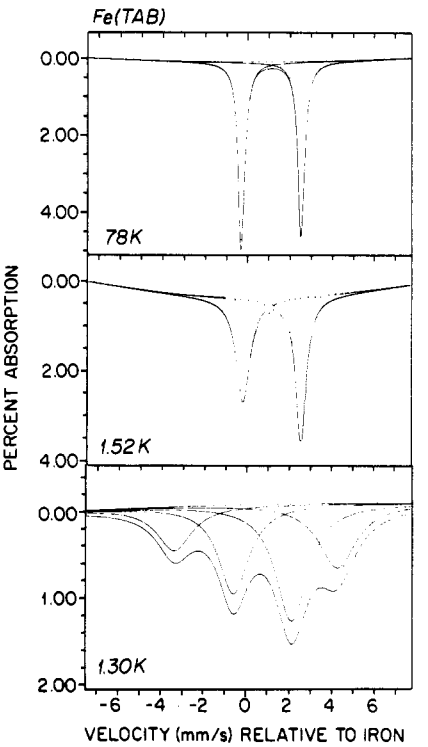

Figure 3. Mössbauer spectra of a polycrystalline sample of FeTAB taken in zero field at 78, 1.52, and 1.30 K.

Mössbauer Spectroscopy. The spectrum of a polycrystalline sample in the paramagnetic state at 78 K (Figure 3) corresponds to a well-resolved quadrupole doublet typical of high-spin iron (II) (isomer shifts and quadrupole splittings ΔE_Q are given in Table V). The spectrum of FeTAB, like that of FeTAC,[5] has a temperature dependence which is remarkably similar to that of the well-studied $FeCl_2 \cdot 2H_2O$. Detailed analysis[22] of the temperature

(21) Takács, L.; Takács, J.; Reiff, W. M.; Ramsden, J. D. *Rev. Sci. Instrum.* **1986**, *57*, 605.

Table V. Isomer Shifts, Quadrupole Splittings, and Internal Magnetic Fields for the Mössbauer Spectra of $[(CH_3)_3NH]_3FeBr_3 \cdot 2H_2O$

T, K	isomer shifts (δ),[a] mm/s	quadrupole splittings (ΔE_Q), mm/s	H_{int}, T
298	1.04	2.55	
77	1.16	2.80	
1.52	1.17	2.73	
1.30	...	...	21.6
1.02	...	...	25.8
0.52	...	...	26.1
0.40	...	...	26.8

[a] Relative to natural iron metal.

dependence of the $FeCl_2 \cdot 2H_2O$ spectrum using the approach of Ingalls[23] indicates a (low-symmetry ligand field component) splitting to the t_{2g} manifold on the order of 500 cm^{-1}. The limiting value of the quadrupolar interaction, ≈2.8 mm/s at 77 K, suggests an orbital singlet ground state. Specifically, in view of the local coordination chromophore (a tetragonally compressed *trans*-$FeBr_4O_2$ environment), one predicts an orbital singlet ground state. In tetragonal symmetry this corresponds to a $^5B_{2g}$ ground term based primarily on the real d_{xy} orbital. For this ground state wave function, the expectation value of the operator for the principal component of the electric field gradient tensor is $-(4/7)q\langle r^{-3}\rangle$. This is positive for electron occupation and leads to a positive electric quadrupole coupling constant, since the quadrupole moment of iron-57 is positive. The existence of a positive electric quadrupole coupling constant can in principle be tested with single-crystal Mössbauer spectra, as was done with FeTAC.[5] Measurements in the paramagnetic state taken with the γ-ray propagation direction parallel to the orthorhombic c axis of the chloride (i.e. nearly parallel to the principal axis of the EFG tensor) showed intensity variations of the two transitions in good agreement with the theoretical ratio for a positive electric quadrupole coupling. Due to the absence of suitable single crystals, comparable experiments with FeTAB have not been possible. However, in view of the structural similarities of the two compounds, we believe the results of the single-crystal experiment on the chloride and the analysis of the polycrystalline spectrum of the bromide leave little doubt as to the positive sign of the electric quadrupole coupling in FeTAB.

Mössbauer spectra showing the development of a partially resolved six-line pattern below 1.3 K are shown in Figure 4. We interpret this splitting as an indication of a transition to an ordered state near 1.3 K, consistent with the susceptibility results (vide infra). An alternative explanation suggests the broadening of the spectrum above 1.3 K is the result of single-ion slow paramagnetic relaxation phenomena resulting from a negative zero-field splitting of the single-ion spin quintet manifold leading to a slowly relaxing $m_s = \pm 2$ ground Kramers doublet. Such broadening could also be the result of soliton effects (moving domain boundaries in the present context) in a one-dimensional magnet just above the critical temperature.[24] These possibilities can be unequivocally distinguished only by determination of a considerable number of spectra and detailed line-width analysis, aspects beyond the scope of the present study. Nevertheless, the observed splitting of the spectra, in conjunction with the magnetic susceptibility data, unambiguously point to the existence of a magnetic ordering transition near 1.3 K.

The lowest temperature (zero-field) spectrum (T = 0.52 K; Figure 4) gives clear evidence of a large quadrupolar shift and perturbation of the hyperfine split spectrum. The quadrupolar shift can readily be determined from the spectrum as the difference $s_1 - s_2$, where s_1 and s_2 are the splittings shown in Figure 4. For

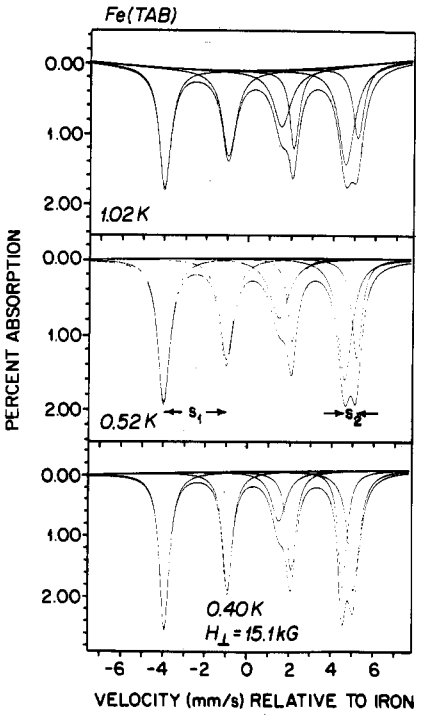

Figure 4. Mössbauer spectra of a polycrystalline sample of FeTAB taken in zero field at 1.02 and 0.52 K, and in a transverse magnetic field of 1.51 kG at 0.40 K. s_1 and s_2 define the quadrupolar shifts defined in the text (eq 1). The solid line corresponds to a simulation of the data with the parameters given in the text.

an axially symmetric EFG tensor, the quadrupolar shift is related to the quadrupole splitting, ΔE_Q, of the paramagnetic phase by

$$s_1 - s_2 = (-\Delta E_Q)(3\cos^2\theta - 1) \quad (1)$$

where θ is the angle between the principal axis of the electric field gradient tensor (V_{zz}) and the internal hyperfine field, with the latter also the direction of the easy axis of magnetization for the ordered state. Since V_{zz} has been shown to be positive by the arguments above, one can calculate the angle θ from the combined interaction spectrum at 0.52 K by using measured values for the difference $(s_1 - s_2)$ and ΔE_Q from the paramagnetic phase. The value for θ from this calculation is 13° away from 90° (either 77° or 103°), placing the local field close to lying within the $FeBr_4$ planes (i.e., within the crystallographic *ab* planes). In comparison, the value of θ found for FeTAC was slightly larger, at 20° away from 90°. This difference will be returned to at the close of the Discussion.

Finally, we refer to the applied field spectrum at the bottom of Figure 4. Save for sharpening and a slight intensification of the $\Delta m_I = 0$ transitions, the applied field has little effect. This indicates the system has likely reached saturation magnetization at 0.4 K. The chloride analogue FeTAC has been shown[5] to undergo a metamagnetic phase transition, with a critical field near 90 G. For such low critical fields, one has little hope of observing the field-induced transition in the spectrum of a single-crystal sample, much less in that of a polycrystalline sample studied here.

The limiting internal hyperfine field for FeTAB is 258 kOe, significantly larger than the values of 200 and 240 kOe found for FeTAC[5] and $FeCl_2 \cdot 2H_2O$,[22] respectively. All of these values are well below the expected value of 440 kOe due to a Fermi contact contribution for four unpaired spins for S = 2 high-spin iron(II). The reduced value is in part the result of a large orbital contribution to the internal hyperfine field, which generally opposes the Fermi contact contribution. Other effects that can reduce the internal field are covalency delocalization and zero-point spin reduction.[25]

(22) Johnson, C. E. *Proc. Phys. Soc.* **1966**, *88*, 943. Chandra, S.; Hoy, G. R. *Phys. Lett.* **1966**, *22*, 254.
(23) Ingalls, R. *Phys. Rev.* **1962**, *128*, 1155.
(24) Thiel, R. C.; de Graff, H.; de Jongh, L. J. *Phys. Rev. Lett.* **1981**, *47*, 1415.
(25) Thomas, M. F.; Johnson, C. E. In *Mössbauer Spectroscopy*; Dickson, D. P. E., Berry, F. J., Eds.; Cambridge University Press: Cambridge, England, 1986; p 179.

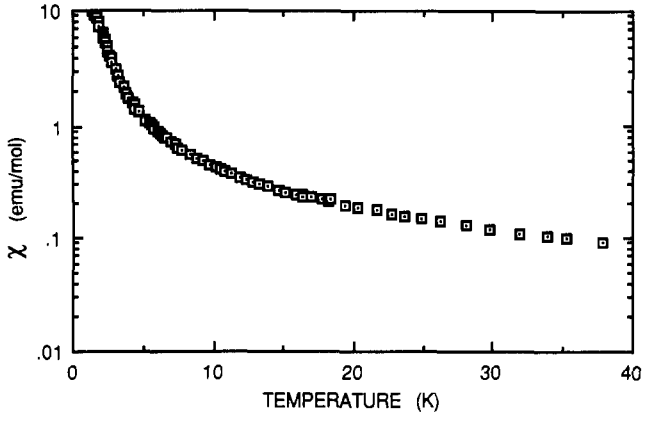

Figure 5. Magnetic susceptibility of a polycrystalline sample of FeTAB plotted versus temperature on a semilogarithmic scale.

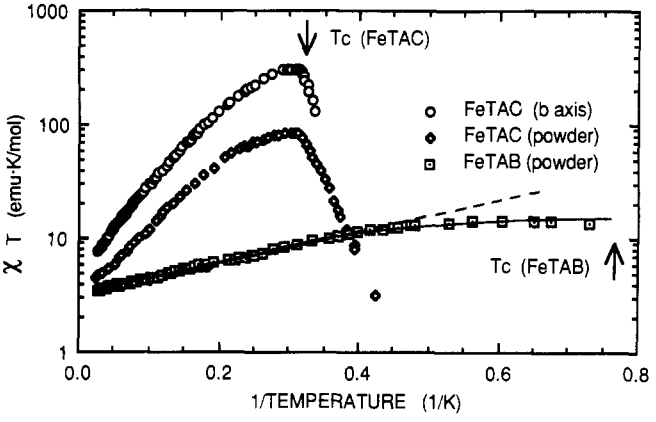

Figure 6. Ising plot (ln (χT) vs T^{-1}) of FeTAB (powder) and FeTAC (powder and single crystal) data. For the FeTAB data, the dashed line shows to fit to the one-dimensional Ising model for $\chi_\parallel$ (eqs 2 and 3), and the solid line shows the fit with the mean field correction (eq 4). The arrows mark the critical temperatures of the two compounds.

Magnetic Susceptibility. The low-temperature magnetic susceptibility of a polycrystalline sample of FeTAB is plotted on a logarithmic scale versus temperature in Figure 5. The susceptibility increases with decreasing temperature at a rate significantly greater than the T^{-1} dependence of the Curie law, indicating the existence of ferromagnetic interactions. Such ferromagnetic interactions were also apparent in the Curie–Weiss fit to the high-temperature data (77–300 K), which yielded best fit parameters C = 3.50 (5) emu K/mol and Θ = +5.5 (5) K. The susceptibility continues to diverge to the lowest temperature reached in the magnetometer cryostat, 1.37 K. At this temperature the susceptibility is 9.94 emu/mol, 2 orders of magnitude greater than its value at 40 K. Although no maximum has been observed for the susceptibility, χ, the product χT does have a maximum value of 14.3 emu K/mol at T = 1.66 K (Figure 6), indicating the onset of the influence of antiferromagnetic interactions.

The appropriate model for the interpretation of the low temperature susceptibility data must take into consideration the special structural features of the TAC/TAB family, i.e. the well-developed superexchange pathways down the chain axes and the relatively good isolation of the chains. A one-dimensional magnetic model is therefore an appropriate starting choice. Whether the exchange model should be isotropic (Heisenberg-like) or axial (Ising-like) cannot be decided a priori; it is necessary to examine the quantitative behavior of the data. Considering the extreme anisotropy found in the magnetic behavior in FeTAC, the one dimensional Ising model is plausible.

The expressions for the parallel and perpendicular susceptibilities of a 1d Ising model have been derived by Fisher[26] based on the spin Hamiltonian $H = -2J\sum_{i,j} S_i^z S_j^z$. The expression for $\chi_\parallel$ is

$$\chi_\parallel = [C_\parallel/T] \exp(J_b/kT) \quad (2)$$

where J_b refers to the exchange down the b (chain) axis. Rearranging eq 2 gives

$$\ln(\chi_\parallel T) = (J_b/k)T^{-1} + \ln(C_\parallel) \quad (3)$$

which is a convenient form to analyze the easy axis susceptibility of a one-dimensional Ising system. The product $\chi_\parallel T$ will appear as a straight line when plotted on a semilogarithmic scale as a function of T^{-1} with the slope equal to the exchange constant and the y-axis intercept equal to the Curie constant. We refer to this type of graph as an Ising plot. Figure 6 is an Ising plot of the powder susceptibility data for FeTAB. For purposes of comparison, FeTAC powder data and easy axis single-crystal data are included on the same plot. It is seen that each of the data sets in Figure 6 does show a linear rise in the product χT corresponding to axial systems with ferromagnetic correlations. The one-dimensional Ising model is therefore the appropriate choice for FeTAB, since Heisenberg systems do not yield straight lines on Ising plots. The two plots for FeTAC show approximately the same slope, corresponding to the same ferromagnetic exchange constant previously determined[5] to be $J_b(\mathrm{Cl})/k$ = 17.4 K. The y-axis intercepts are quite different for the two FeTAC curves since the powder data yields an average value for the Curie constant, $C_{av} = (C_a + C_b + C_c)/3$ = 2.7 emu K/mol, while the single crystal data gives the Curie constant measured along the easy axis, C_b = 5.2 emu K/mol. The FeTAB data, on the other hand, show a linear rise but with a considerably smaller slope, indicating a weaker intrachain exchange constant. The y-axis intercepts are similar for both powder data sets, indicating the average Curie constants are approximately the same for the two compounds.

Fitting the FeTAB data to eq 3 over the temperature range 3–40 K yields best-fit parameters $J_b(\mathrm{Br})/k$ = 3.2 (1) K and C = 3.25 (3) emu K/mol. For this procedure C is actually $C_{av} = [C_\parallel + 2C_\perp]/3$. The quality of the fit is good, with no differences greater than 4% found; most of the data are in much better agreement. So long as the data is confined within the temperature range cited (corresponding to the linear region of the Ising plot), neither the quality of the fit nor the values of the parameters are affected by the upper or lower temperatures of the range.

Comparison of powder susceptibility data to an expression for the parallel susceptibility is not exact. More correctly, the powder susceptibility should be compared to the expression $[\chi_\parallel + 2\chi_\perp]/3$, where the Curie constants for the parallel and perpendicular susceptibilities are independent parameters. Attempts to model the FeTAB data to this combination always led to a value of zero for the Curie constant of the perpendicular susceptibility. The same result was also observed when fitting the powder FeTAC data. It is known from the previous single-crystal studies on both CoTAC[7] and FeTAC[5] that the parallel susceptibility can be several orders of magnitude greater than the perpendicular susceptibilities, so the above result is not surprising. In any case, the exchange constants obtained from fitting both the powder and single crystal data of FeTAC to eq 3 agree to within 4%, so the error in neglecting the contribution of $\chi_\perp$ is not large.

Deviations from linear behavior in the Ising plot correspond to the influence of interchain interactions. For FeTAC these are downward and lead to a sharp break in the data at the ordering temperature T_c = 3.14 K (T^{-1} = 0.32 K^{-1}). For FeTAB, the deviations are also downward, but a sharp break indicative of the onset of long-range order is not yet seen. Judging from the Mössbauer results, such a break should appear near 1.3 K (0.77 K^{-1}) as indicated by the arrow in Figure 6. In both cases, the downward curvature of the data sets on the Ising plot corresponds to net antiferromagnetic interchain exchange, since its effect is to slow the rate of divergence of the ferromagnetic susceptibility.

A mean field correction to the one-dimensional Ising model has previously been used[6] to quantitatively characterize the deviations (curvature) from the ideal (linear) behavior of the susceptibility

(26) Fisher, M. E. *J. Math. Phys.* **1963**, *4*, 1963.

data in Figure 6 in terms of the net interchain magnetic interaction $z'J'$.

$$\chi_{MF} = \chi_{1d}(1 - z'J'\chi_{1d}/2Ck)^{-1} \quad (4)$$

In this case χ_{1d} is $\chi_{\parallel}$ from eq 2, and C is C_{av}. The entire FeTAB data set from 1.37 to 40 K can be fit well to eq 4 by varying the three parameters J/k, $z'J'$, and C_{av} (solid line in Figure 6). The best fit parameters are $J_b/k = 4.09$ (6) K, $z'J'/k = -0.43$ (1) K, and $C_{av} = 3.06$ (2) emu K/mol.

The magnitude of $z'J'$ is overestimated when eq 4, written in terms of the parallel susceptibility, is applied to powder data; we believe the true value of $z'J'$ in interchain interactions in FeTAB to be smaller than that obtained from the above procedure. To test the equation, we have applied eq 4 to FeTAC, where both powder and single-crystal data are available (Figure 6). When the FeTAC powder data are fit, a value of $z'J'(Cl)/k = -0.15$ K is obtained. However, the single crystal data for $\chi_{\parallel}$ yield a value that is a factor of 2 smaller, $z'J'(Cl)/k = -0.08$ K. Evidently the inclusion of the (smaller) contributions from the perpendicular components of the powder susceptibility leads to an artifically large value for the antiferromagnetic interchain exchange constant. The more likely value for the interchain interactions in FeTAB based upon the molecular field correction is therefore $z'J'(Br)/k \approx -0.2$ K.

An alternative procedure for the determination of $z'J'$ is based upon the theoretical prediction[27] for the dependence of the ordering temperature of an three-dimensional array of ferromagnetic Ising linear chains by Chalupa and Novotny. Their model was a CoTAC-like system in which ferromagnetic Ising chains are coupled in one transverse direction by a ferromagnetic interaction J_F and in the other direction by an antiferromagnetic interaction J_A. Both J_F and J_A are absolute magnitudes. Exact expressions were used for the correlations within the chains, whereas the coupling between the chains through J_F and J_A was done in the mean field approximation. An expression for the sum of the interchain exchange constants in terms of the ordering temperature T_c in zero field was found to be

$$|z_cJ_c/k| + |z_aJ_a/k| = 2T_c/[\exp(J_b/kT_c)] \quad (5)$$

where the substitutions $|z_cJ_c/k| = 2J_F$ and $|z_aJ_a/k| = 2J_A$ have been made. Substituting the known values of T_c and J_b for CoTAC and FeTAC produces the result that $|z_cJ_c/k| + |z_aJ_a/k| = 0.308$ K for CoTAC and 0.024 K for FeTAC. This value for CoTAC is in excellent agreement with the published result[7] (Table VI) of 0.312 K. The value for FeTAC is a factor of 3 smaller than that obtained from eq 4, even when the single-crystal data are used. When eq 5 is applied to FeTAB, a value of 0.12 K is obtained for the sum of the absolute values of the interchain exchange constants, roughly a factor of 2 smaller than the estimate for $z'J'$ based upon the molecular field correction to the susceptibility.

In summary, there remains doubt as to the precise value of J' in FeTAB, due to the absence both of single-crystal data and of an exact theory for the dependence of the ordering temperatures of one-dimensional systems upon the J'/J ratio. Nevertheless, it is certain that the sign of $z'J'$ in FeTAB is negative and that the magnitude most likely lies between 0.1 and 0.2 K. The ratio $z'J'/J_b$ for FeTAB is therefore between 0.025 and 0.05, far greater than the value of 0.0026 found for FeTAC and somewhat greater than the value of 0.019 for CoTAC (Table VI).

The effect of the J'/J_b ratio is displayed graphically in Figure 7, where the FeTAC and FeTAB data are plotted on an Ising plot with a relative temperature scale of J_b/kT. From eq 3, it is clear that all pure Ising ferromagnetic chains should have the same slope on this curve; any differences seen are therefore attributable to the differing amounts of interchain interactions in the two compounds. It is observed that both the deviations from linearity and the transition to three-dimensional ordering appear at a much higher relative temperature in the FeTAB curve. The critical temperature ratios (kT_c/J_b) for FeTAB and FeTAC are 0.33 and 0.18, respectively. By comparison, the critical temperature ratio for the analogous cobalt compound, CoTAC, is 0.30. These trends are consistent with the theoretical predictions of eq 5, in which the critical ratio is shown to have a weak logarithmic dependence on the ratio J'/J_b.

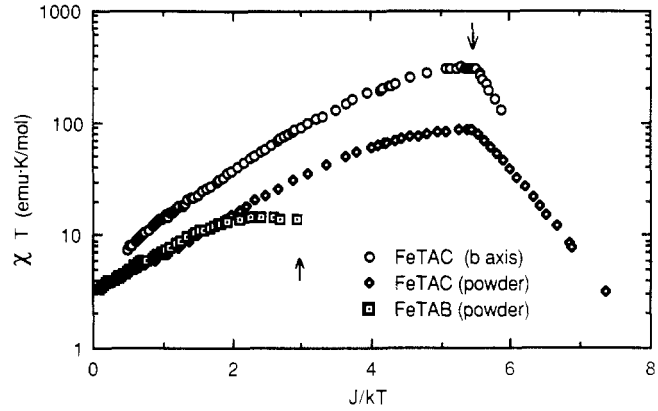

Figure 7. Reduced Ising plot (ln (χT) vs J/kT) of FeTAB (powder) and FeTAC (powder and single crystal) data. Data sets for Ising systems with the same J'/J ratio will show identical deviations from linearity and the same (reduced) critical temperature. The arrows mark the reduced critical temperatures of the two compounds.

Magnetostructural Correlations. FeTAB is therefore characterized by both a considerably smaller intrachain exchange and a much larger ratio of interchain to intrachain exchange than that found for FeTAC. What explains these differences? Considering first the interchain exchange, we note from Table VI that the absolute magnitude of the net interchain exchange in FeTAB, $|z'J/k| \approx 0.2$ K, is not unusually low, compared to those for the other TAB/TAC members. The values for the non-ferrous members range from a high of 0.74 K for MnTAB to a low of 0.15 K for NiTAC. The exception is FeTAC, whose value of 0.04 K is a factor of 4 lower than any other.

The interchain interactions in the c direction have usually been attributed to a superexchange pathway involving hydrogen bonding from the water molecules to the lattice halide X(3). A second possibility is direct halide–halide overlap between the halide ions in the chain and the lattice halide. Either mechanism is expected to lead to an increase in J' when passing from FeTAC to FeTAB.

As mentioned in the structural description, the separation of the chains along c is only 0.18 Å greater for FeTAB, whereas the increase in ionic radii would predict an increase of separation of 0.6 Å. The bromide system is therefore considerably more compressed along c than expected, as can be seen in the X(1)–X(3) distances (4.098 Å, Cl; 4.188 Å, Br; 4.052 Å, Cl; 4.149 Å, Br). Less than one-third of the expected increase of 0.3 Å is found here as well. Both of these effects will lead to a more effective superexchange pathway between the chains and to an enhanced J'.

The same effect is apparent for the manganese pair of compounds. While only the lattice parameters have been reported for MnTAB[4] ($a = 17.21$ Å, $b = 7.57$ Å, $c = 8.51$ Å), they do show the increase in the c-axis parameter (0.31 Å) to be only half the expected increase. As in the case of the ferrous compounds, the value of $z'J'/k$ shows an increase of approximately 0.2 K when going from MnTAC to MnTAB (Table VI).

Turning now to the intrachain exchange constant, examination of Table VI shows that the effect of bromine substitution upon J_b has been small for other members of the TAC/TAB family. The exchange parameter of MnTAB is −0.41 K, slightly larger than the value of −0.36 K seen in MnTAB. The results for CoTAB have never been reported in detail, but passing reference is made[16] to the material being virtually identical with the chloride analogue. The decrease in exchange strength from 17.4 to 4 K for FeTAC/FeTAB is therefore unprecedented.

There are several possible explanations for this decrease, having their origins in either the geometrical or chemical differences between the compounds. The geometrical differences consist of bond distances and angles. The metal–metal distance has ex-

(27) Chulapa, J.; Novotny, M. A. *Solid State Commun.* **1985**, *54*, 843.

Table VI. Magnetic Parameters for Members of the Series $[(CH_3)_3N]MX_3 \cdot 2H_2O$ (M = Metal, X = Cl, Br)

param	MnTAC	MnTAB	FeTAC	FeTAB	CoTAC	CoTAB	NiTAC	CuTAC
exchange anisotropy[h]	H	H	I	I	I	I	H	H
J_b/k, K	−0.36	−0.41	17.4	4	13.8	≈13	14.0	0.85
$z'J'/k$, K	−0.55	−0.74	−0.046	−0.2	0.26		0.11	−0.24
$\lvert z'J'/J_b \rvert$	1.5	1.8	0.0026	0.05	0.019		0.008	0.28
T_c, K	0.98	1.56	3.14	1.3	4.18	3.86	3.67	0.165
$kT_c/\lvert J \rvert$	2.72	3.80	0.18	0.33	0.30	≈0.30	0.26	0.19
$kT_c/\lvert J \rvert S(S+1)$	0.31	0.43	0.24	0.43	0.40	≈0.40	0.13	0.25
ref	*a,b*	*a,b*	*c*	this work	*d*	*e*	*f*	*g*

[a] Merchant, S; McElearney, J. N.; Shankle, G. E.; Carlin, R. L. *Physica* **1974**, *78*, 308. [b] Takeda, K.; Koike, T.; Harada, I.; Tonegawa, T. *J. Phys. Soc. Jpn.* **1982**, *51*, 85. [c] Greeney, R. E.; Landee, C. P.; Zhang, J. H.; Reiff, W. M. *Phys. Rev. B: Condens. Matter* **1989**, *39*, 12200. [d] Groenendijk, H. A.; van Duyneveldt, A. J. *Physica B + C*, **1982**, *115*, 41. [e] Carlin, R. L. *Magnetochemistry*; Springer-Verlag: Berlin, Heidelberg, FRG, New York, Tokyo, 1986; p 218. [f] Hoogerbeets, R.; Wiegers, S. A. J.; van Duyneveldt, A. J.; Willett, R. D.; Geiser, U. *Physica B + C* **1984**, *125*, 135. [g] Algra, H. A.; de Jongh, L. J.; Huiskamp, W. J.; Carlin, R. L. *Physica B + C* **1977**, 187. [h] I = Ising; H = Heisenberg.

panded from 3.68 Å (Cl) to 3.83 Å (Br). The Fe–X(*i*)–Fe bridging angles are also smaller, Fe–X(1)–Fe decreasing from 95.5 to 93.9°, and Fe–X(2)–Fe decreasing from 92.7 to 90.5° when chloride is changed to bromide. In addition, the dihedral fold angle between adjacent FeX_4 planes has increased in the bromide, to 19.8° from 16.3°. However, these changes are consistent with the effect of the enlargement of the halide ion. Similar structural changes must have occurred in the chains of MnTAB and CoTAB, yet little shift has been observed in their values of J_b.

The chemical differences lie in the dependence of the superexchange interaction upon the energy levels of the specific ligand ions. As discussed by Willett,[17] the Hoffmann description of superexchange[28] expresses the exchange due to a given orbital as

$$2J = 2J_F - (\epsilon_s - \epsilon_a)^2/(J_{aa} - J_{ab})$$

where J_{aa} and J_{bb} are one- and two-center Coulomb integrals ($J_{aa} > J_{ab}$), and ϵ_s and ϵ_a are the one electron energies of the symmetric and antisymmetric combination of magnetic orbitals on the two metal centers. The antiferromagnetic contribution to the exchange therefore is proportional to the square of the difference between the one electron energies. Hay et al.[28] argue that the difference $\epsilon_s - \epsilon_a$ is inversely proportional to the difference in energies between the ligand orbitals and the magnetic orbital on the metal. An estimate for this latter energy difference can be obtained from the ligand-to-metal charge-transfer bands. For the simplified case of the copper(II) halides with only one magnetic orbital, Willett has demonstrated a good correlation between the smaller ligand–metal energy difference and the enhanced antiferromagnetic contribution of the compounds involving the less electronegative bromide ion.[17]

In principle, the Hoffmann formalism can be applied to metal ions with more than one magnetic electron, the net exchange simply being the sum of the contributions from the individual orbitals. We therefore anticipate that the less electronegative bromide ion will once again lead to smaller charge-transfer energies and a greater antiferromagnetic contribution to the exchange interaction, as observed. Confirmation of this hypothesis though spectroscopic examination of the charge-transfer bands has not been possible, due to the lack of adequate samples. In any case, the same argument should lead to more antiferromagnetic exchange in the manganese and cobalt bromides, which is not observed.

The difference between the interaction exchange constants of FeTAC and FeTAB therefore remains unexplained at this time. Neither the geometry nor the chemistry can offer a simple explanation that does not apply equally as well to the manganese and cobalt systems. The final explanation must consider in detail the specific magnetic orbitals occupied by each of the metal ions and the dependence upon the superexchange of changes of both geometry and ligand chemistry. It is clear that the FeTAC/FeTAB system offers a much more sensitive test of calculations than any other member of this family.

(28) Hay, P. J.; Thibeault, J. C.; Hoffmann, R. *J. Am. Chem. Soc.* **1975**, *97*, 4884.

Assessment of the magnetic anisotropy within FeTAB awaits the availability of single crystals. However, the powder Mössbauer spectra do provide one point of comparison to FeTAC. Spin canting has been predicted to be present in FeTAC, due to the presence of the 2_1 screw axis parallel to *b*. Comparison of the structures and Mössbauer spectra of FeTAC and $\cdot FeCl_2 \cdot 2H_2O$ indicated the local easy axis for FeTAC lies parallel to the Fe–Cl(1) bond. Since there are two inequivalent Fe–Cl(1)'s within the chains, the local easy axes are canted. The effect of the ferromagnetic exchange interaction J_b is to pull the moments toward a parallel configuration. The remnant canting angle depends on the competition between the exchange and anisotropy fields. As referred to in the section on the Mössbauer spectra, the quadrupolar shifts indicate that the angle θ between the principle axis of the EFG and the local easy axis was 20° different from 90° for FeTAC. Such as difference is a natural consequence of the moments being pulled parallel to the *b* axis and out of the $FeCl_4$ planes by the exchange interaction.

For FeTAB, the angle θ has been shown to be only 13° away from 90°; this corresponds to a smaller tilting out of the $FeBr_4$ planes. This value is consistent with the larger limiting hyperfine field seen in FeTAB (250 kOe) and the weaker value for J_b. The weaker exchange field will have less effect against the stronger hyperfine field and the moments will remain more closely aligned with the local easy axis. We may therefore conclude that the canting within the chains of FeTAB will be more exaggerated than in FeTAC.

Summary

FeTAB has been shown to be isostructural with other members of the TAC/TAB family. The ferromagnetic interactions within the chain ($J_b \approx 4$ K) are one-fourth as strong as those found for the chloride analogue. The interactions between the chains ($z'J'/k \approx 0.2$ K) are in the normal range for these compounds but 30 times greater than that seen in FeTAC. Mössbauer spectra indicate an ordering transition near 1.3 K. Analysis of the spectra shows that the internal magnetic field lies close to the $FeBr_4$ planes and leads to a prediction of significant spin canting within the chains.

Acknowledgment. This research was supported in part by NSF Grants DMR-8306432 (C.P.L.) and DMR-8313710 (W.M.R.). We also acknowledge the Northeastern University Biomedical Research and Research and Scholarship Development funds for monies that purchased the Co^{57} source. The magnetometer was purchased with a grant from the NSF College Research Instrumentation Program. We thank R. D. Willett and Brian Scott for the crystal structure determination and for helpful discussions about magnetochemical correlations. Professor Willett's work was supported in part by NSF Grant CHE-8408407. The X-ray diffractometer system was purchased in part with a grant from the Boeing Co. C.P.L. thanks his colleagues at the Laboratorie de Physique des Solides, Université de Paris-Sud, for their hospitality during the preparation of the manuscript.

Supplementary Material Available: Tables SI–SIII, listing complete data collection parameters, anisotropic thermal parameters for non-hydrogen atoms, and hydrogen atom positional and isotropic thermal parameters (4 pages); tables of calculated and observed structure factors (8 pages). Ordering information is given on any current masthead page.